Role of convective cell in nonlinear interaction of kinetic Alfvén waves

O. O. Luk and Z. Lin[a)]
University of California, Irvine, California 92697, USA

(Received 24 June 2016; accepted 20 September 2016; published online 11 October 2016)

Gyrokinetic particle simulations show that electrostatic convective cell (CC) can be generated by kinetic Alfvén waves and plays a dominant role in the nonlinear interactions underlying perpendicular spectral cascade. The CC growth rate increases linearly with the field amplitude of the pump waves and has a small but finite threshold, and decreases with the parallel wavevector. The CC growth is proportional to the perpendicular wavevector when there are two pump waves, but proportional to the square of the perpendicular wavevector when there is a single pump wave. *Published by AIP Publishing.* [http://dx.doi.org/10.1063/1.4964146]

I. INTRODUCTION

The nonlinear interactions of Alfvén waves cause wave energy to cascade, which is anisotropic by observation,[1,2] through the intermediate spatial scale, and then dissipate to the background plasma through smaller spatial scale. Theoretical and numerical attempts were made to understand this anisotropic cascade,[3–5] which may be caused by the magnetic field.[6–10] At a high frequency and spatial scale of approximately the size of ion gyroradius, the spectrum at the dissipation range steepens.[11–13] Many hypotheses to explain the steepened power spectrum at dissipation range were proposed. These include ion cyclotron damping,[14] Landau damping of kinetic Alfvén wave (KAW),[15] stochastic heating by dispersive Alfvén waves,[16,17] weakly damped magnetosonic and whistler waves.[18–20]

The basic nonlinear process underlying the Alfvén cascade is three-wave coupling that leads to parametric decay instability.[21,22] A possible mechanism preferring perpendicular cascade is the generation of convective cell (CC). The CC is a two-dimensional plasma wave traveling in the direction perpendicular to the magnetic field (parallel wavevector $k_{\|} = 0$).[23] It is possible that the parametric instability of KAW generates CC. The coupling of CC with KAW could then lead to turbulence in the upper ionosphere.[24,25] Furthermore, the large-scale CC could disrupt KAW turbulence and therefore contributes to the evolution of ionospheric plasma turbulence.[26]

There are two types of CC: electrostatic (ESCC) and magnetostatic (MSCC). The ESCC can be described by the zonal component ($k_{\|} = 0$) of scalar potential; they could drive macroscopic plasma convection.[23,27,28] On the other hand, the MSCC can be described by the zonal component of vector potential; they are tied to magnetic-field bending.[23,29,30] The KAW can excite ESCC and MSCC at the same time, but only at a short-wavelength limit.[31,32] This process could lead to diffusive isotropization of the perpendicular KAW spectrum. A 3-dimensional ion particle simulation found that a mode with $k_{\|} = 0$ gets excited during parametric decay instability, which may be related to the wave energy transfers to larger $k_{\perp}$ modes to drive large transport across plasma boundaries.[33] A subset of CC is the zonal field, which is perturbation dependent only of magnetic flux surfaces.[34] A global gyrokinetic particle simulation[35] demonstrates that the zonal flow could reduce transport and regulate the driftwave turbulence in fusion plasma.

The objective of this paper is to understand the role of CC in the nonlinear interaction of KAW that leads to the perpendicular cascade of the spectral energy. As emphasized in the earlier theory and simulation,[22,31–34] CC generation by KAW depends quantitatively and qualitatively on kinetic effects (such as finite Larmor radius (FLR) and wave-particle interactions) that break the ideal MHD in purely Alfvénic state. Therefore, a kinetic approach such as gyrokinetic simulation is required for studying the CC generation and dynamics. Particle simulation results show that a pump wave energy cascades to waves of shorter wavelengths during KAW interactions. There are three (including a CC) among these daughter waves, which are essential in producing the energy cascade of a single standing pump wave. In particular, ESCC was found to play a major role in the nonlinear KAW interaction. The CC growth rate increases linearly with the field amplitude of the pump wave and has a small but finite threshold. It is proportional to the square of the perpendicular wavevector and reduced by the parallel wavevector. In the simulations of two pump waves, we observed that a CC growing exponentially satisfies the wave-matching condition and the nonlinear $E \times B$ convection in the KAW interactions. The CC growth rate is linearly proportional to the perpendicular wavevector.

The rest of this paper will be displayed in the following order: Section II introduces the simulation model. Section III shows the simulation results on the role CC plays during KAW interaction. Section IV summarizes simulation results and discusses future work.

II. SIMULATION MODEL

We are interested in studying KAWs that have a frequency ω much lower than the ion cyclotron frequency ($\Omega_i \equiv eB_0/m_i/c$) due to strong background magnetic field. Here, e is the ion charge, B_0 is the background magnetic field strength, m_i is the ion mass, and c is the speed of light. The

[a)]Author to whom correspondence should be addressed. Electronic mail: zhihongl@uci.edu

spatial scale of background plasmas is much larger than the ion gyroradius. However, the finite Larmor radius (FLR) effects could greatly affect nonlinear physics, since $k_\perp \rho_i \sim 1$, where ρ_i is the ion gyroradius. The compressional modes are not important for low-β (plasma-to-magnetic pressure ratio) plasmas. It is difficult to excite large $k_\parallel$ modes due to field-line bending effects. Therefore, $k_\perp$ is much bigger than $k_\parallel$. We assume that perturbed potential energy and perturbed magnetic field strength δB is much smaller than kinetic energy and B_0, respectively.

A. Gyrokinetic formulation

The KAW and CC can be most efficiently studied using nonlinear gyrokinetic theory,[36] which eliminates the uninteresting gyro-motion of ions by averaging over cyclotron orbit, while keeping all low-frequency interesting physics. In gyrokinetic theory, the orderings are

$$\frac{\omega}{\Omega_i} \sim \frac{\rho}{L} \sim k_\parallel \rho_i \sim \frac{e\delta\phi}{T_e} \sim \frac{\delta B}{B_0} \sim \epsilon, \quad k_\perp \rho_i \sim 1, \tag{1}$$

where ρ is the length scale of the wave of interest, L is the equilibrium scale length of the magnetic field, $\delta\phi$ is the perturbed scalar potential, T_e is the electron temperature, and ϵ is the smallness number. In this work, the background plasma is assumed to have a uniform magnetic field $\mathbf{B}_0 \equiv B_0 \mathbf{b}_0$, particle density n, and temperature T.

In the gyrokinetic theory, the phase space coordinates are transformed from particle coordinates $(\mathbf{x}, \mathbf{v})$ to gyrocenter coordinates $(\mathbf{X}, \mu, v_\parallel, \theta)$, where $\mathbf{x}$ is particle position, $\mathbf{v}$ is the particle velocity, $\mathbf{X}$ is the gyrocenter position, μ is the magnetic moment, $v_\parallel$ is the gyrocenter velocity along the magnetic field and θ is the gyroangle. With the transformed coordinate system, the gyroangle-averaged Vlasov equation becomes the nonlinear gyrokinetic equation for species α[36]

$$\left(\frac{\partial}{\partial t} + \dot{\mathbf{X}} \cdot \nabla + \dot{v_\parallel} \frac{\partial}{\partial v_\parallel}\right) f_\alpha(\mathbf{X}, \mu, v_\parallel, \theta) = 0, \tag{2}$$

where f_α is the gyrocenter distribution function for the species α. More specifically

$$\dot{\mathbf{X}} = v_\parallel \frac{\mathbf{B}}{B_0} + \mathbf{v}_\mathbf{E}, \tag{3}$$

$$\dot{v_\parallel} = -\frac{q_\alpha}{m_\alpha}\left(\frac{\mathbf{B}}{B_0} \cdot \nabla \delta\phi + \frac{1}{c}\frac{\partial}{\partial t}\delta A_\parallel\right). \tag{4}$$

Here $\mathbf{B} \equiv B\mathbf{b} = \mathbf{B}_0 + \delta\mathbf{B}$ as total magnetic field, $\delta\mathbf{B}$ as perturbed magnetic field, $\mathbf{v}_\mathbf{E}$ as $E \times B$ drift, $\delta A_\parallel$ represents the vector potential along $\mathbf{B}_0$. m_α and q_α as the particle mass and charge of species α, respectively.

We also made the assumption that δB has no compressional component for $\beta \ll 1$. Therefore, $\delta\mathbf{B}$ can be expressed as $\delta\mathbf{B} \approx \delta\mathbf{B}_\perp \approx \nabla_\perp \times \delta\mathbf{A}_\parallel$. The gyrocenter distribution function for species α could be expanded to distinguish equilibrium distribution and perturbed distribution: $f_\alpha = f_{0\alpha} + \delta f_\alpha$. Here, $f_{0\alpha}$ is the distribution of background and satisfies the equilibrium equation: $v_\parallel \mathbf{b}_0 \cdot \nabla f_{0\alpha} = 0$. $f_{0\alpha}$ is uniform in real space and Maxwellian in velocity space

$$f_{0\alpha} = \frac{n_{0\alpha}}{(2\pi T_{0\alpha}/m_\alpha)^{3/2}} \exp\left(\frac{-2\mu B_0 - m_\alpha v_\parallel^2}{2T_{0\alpha}}\right). \tag{5}$$

The δf_α is the perturbed distribution function for species α.

In the nonlinear gyrokinetic simulation, the perturbed particle distribution is governed by the gyrokinetic equation

$$\left(\frac{\partial}{\partial t} + \dot{\mathbf{X}} \cdot \nabla + \dot{v_\parallel}\frac{\partial}{\partial v_\parallel}\right)\delta f_\alpha = -\dot{v_\parallel}\frac{\partial}{\partial v_\parallel} f_{0\alpha}. \tag{6}$$

In the perturbative (δf) simulation, ion weight w_i is defined to represent the perturbed distribution function $w_i \equiv \delta f_i / f_i$. The dynamic expression for w_i can be expressed using gyroaveraged scalar potential $\langle\delta\phi\rangle$ and gyroaveraged vector potential $\langle\delta A_\parallel\rangle$

$$\frac{\mathrm{d}w_i}{\mathrm{dt}} = -(1 - w_i)\frac{e}{m_i}\frac{v_\parallel}{v_i^2}\left(\nabla_\parallel\langle\delta\phi\rangle + \frac{1}{c}\frac{\partial}{\partial t}\langle\delta A_\parallel\rangle\right). \tag{7}$$

v_i is the ion thermal speed.

B. Electron model

The electron dynamics are hybrid, with the 0th order motion treated as a massless fluid and higher orders as kinetic.[37] We treat electrons as a massless fluid in this work because electron beta β_e in our simulation satisfies $\beta_e m_i/m_e \gg 1$, where $v_e \gg v_A \sim v_i$ and thus the ion Landau damping effect is dominant compared to electron Landau damping. Note that v_e is electron thermal speed and v_A is the shear Alfvén wave speed.

In the lowest order of the hybrid electron model, electron responses are adiabatic, $k_\parallel v_e \gg \omega$, then

$$\mathrm{e}^{-e\delta\psi/T_e} = 1 + \frac{\delta n_e}{n_0}. \tag{8}$$

$\delta\psi$ is defined as the effective potential of perturbed parallel electric field

$$-\nabla_\parallel \delta\psi = -\nabla_\parallel \delta\phi - \frac{1}{c}\frac{\partial}{\partial t}\delta A_\parallel. \tag{9}$$

If we integrate Eq. (6) in the velocity space and keep terms of up to the 2nd order, then the time evolution of the electron charge density δn_e can be described by the electron continuity equation

$$\frac{\partial}{\partial t}\delta n_e + n_0 \mathbf{b} \cdot \nabla \delta u_{\parallel e} + \frac{c\mathbf{b}_0 \times \nabla\delta\phi}{B_0} \cdot \nabla \delta n_e = 0, \tag{10}$$

where $\delta u_{\parallel e}$ represents the perturbed parallel electron current density.

C. Field equations

When calculating the field equations, the ion density δn_i and ion current density $n_0 \delta u_{\parallel i}$ are in particle positions.

However, the gyrokinetic equation (Eq. (6)) is defined in gyro-center position. The gyro-averaged ion density and ion current density could be converted from gyro-center position to particle position.

Any field quantity can be found by adding both zonal and nonzonal (NZ) components together. For example, $\delta A_\parallel$ is equivalent to $\delta A_\parallel = \delta A_\parallel^{NZ} + \overline{\delta A_\parallel}$. The dynamic equation that solves for the time evolution of $\delta A_\parallel^{NZ}$ can be obtained with the definition of parallel electric field

$$\frac{1}{c}\frac{\partial}{\partial t}\delta A_\parallel^{NZ} = \mathbf{b}_0 \cdot \nabla\left(\delta\psi - \delta\phi^{NZ}\right). \tag{11}$$

$\delta\phi^{NZ}$ represents the scalar potential and could be solved using the gyrokinetic Poisson's equation[38]

$$\frac{\tau}{\lambda_D}\left(\delta\phi - \delta\tilde{\phi}\right)^{NZ} = 4\pi\sum_\alpha q_\alpha \delta n_\alpha^{NZ}, \tag{12}$$

where $\delta\tilde{\phi}^{NZ}$ is the 2nd gyrophase-averaged potential and δn_α^{NZ} is the particle density of species α that contributes to the NZ scalar potential. τ is the electron-to-ion temperature ratio ($\tau \equiv T_e/T_i$), and λ_D is the Debye length.

D. Zonal fields

The zonal fields are composed of zonal density $\overline{\delta\phi}$ and zonal current $\overline{\delta A_\parallel}$. The overbar represents $k_\parallel = 0$ component. Derivations of $\overline{\delta\phi}$ and $\overline{\delta A_\parallel}$ were shown by Holod *et al.*[39] and Wang[40] in their electromagnetic formulation of the electron hybrid model in toroidal geometry.

$\overline{\delta\phi}$ is very straight-forward to obtain, and it is similar to the expression on $\delta\phi^{NZ}$ (see Eq. (12)). Therefore, $\overline{\delta\phi}$ could be expressed as

$$\frac{\tau}{\lambda_D}\overline{\left(\delta\phi - \delta\tilde{\phi}\right)} = 4\pi\sum_\alpha q_\alpha \overline{\delta n_\alpha}. \tag{13}$$

In Wang's formulation on zonal fields,[40] for $\overline{\delta A_\parallel}$ with scale length k^{-1} larger than electron collisionless skin depth δ_e, the Ampère's law for zonal field is expressed as

$$\overline{\delta A_\parallel} = \frac{4\pi e}{c}\delta_e^2\left(\overline{\int_{GC}\delta f_i v_\parallel d\mathbf{v}} - \overline{\int_{GC}\delta h v_\parallel d\mathbf{v}}\right), \\ -c\int\overline{\frac{\delta B}{B_0}\cdot\nabla\delta\phi}\,dt, \tag{14}$$

where δh is the higher order non-adiabatic response, and GC represents the gyrocenter trajectory. The first term on the right-hand-side of Eq. (14) is parallel current screened by δ_e. The second term is a nonlinear ponderomotive force arising from derivation of ideal MHD. However, this new term does not play a major role to the overall simulation outcome.[40] Since electrons are adiabatic in our simulation, $\delta h = 0$.

The flow velocity $\delta u_{\parallel e}$ can be expressed in the form $\delta u_{\parallel e} = \delta u_{\parallel e}^{NZ} + \overline{\delta u_{\parallel e}}$. Using the gyrokinetic Ampère's law

$$\delta u_{\parallel e} = \left(\delta u_{\parallel i}^{NZ} + \frac{c}{4\pi e n_0}\nabla_\perp^2\delta A_\parallel^{NZ}\right) + \frac{e}{m_e c}\overline{\delta A_\parallel}, \tag{15}$$

where the fluid electron response associated with $\overline{\delta A_\parallel}$ is

$$\frac{4\pi e n_0}{c}\overline{\delta u_{\parallel e}} = \frac{1}{\delta_e^2}\overline{\delta A_\parallel}. \tag{16}$$

III. SIMULATION RESULTS

A. Direction of energy cascade of a pump wave

The plasma in this simulation is composed of gyrokinetic ions and fluid electrons, with $\beta_e = 0.16$ and $\tau = 1.0$. The coordinate system used here is the Cartesian coordinate system, with the z-axis being parallel to $\mathbf{B}_0$. The convergence parameters include a number of particles per (shortest) wavelength $N_p = 6400$, a number of grids $N_g = 64$ for each direction, and a size of each time step $\omega_A\Delta t = 0.049$. $\omega_A = k_\parallel v_A$, where $k_\parallel\rho_s = 0.002$.

To test the energy channel of a KAW into other waves, a pump wave with an initial magnetic field perturbation of $\delta B/B_0 = 0.012$ is introduced into the plasma. This pump wave is a standing wave and has a wavevector of $k_x\rho_s = k_\perp\rho_s = 0.2$, $k_y\rho_s = 0$ and $k_\parallel\rho_s = 0.002$. All other waves have no amplitudes at initial time t = 0. The energy of the pump wave is allowed to transfer into waves with wavevectors 0, 0.5, 1.5, and 2.0 times of the pump wave. A wave along any axis in the Cartesian coordinates with wavelength equal to the size of the simulation box is labeled as mode with index 1, wavelength equivalent to half the size of the simulation box is labeled as mode with index 2, etc. Hence, the pump wave is labeled as wave of mode 202.

As Figure 1 demonstrates, energy transfers mostly to waves with shorter wavelengths. The daughter waves that get the highest growth rate γ are modes 040, 242, and 444. The growth rates of those three dominant modes are displayed in Table I, which shows that their γ are approximately the same. Theoretically all three daughter waves should have identical growth rates due to wave-wave interaction. However, the measured values are slightly different (less than 1%). The discrepancy among growth rates may have to do with the numerical noise or the measurement method.

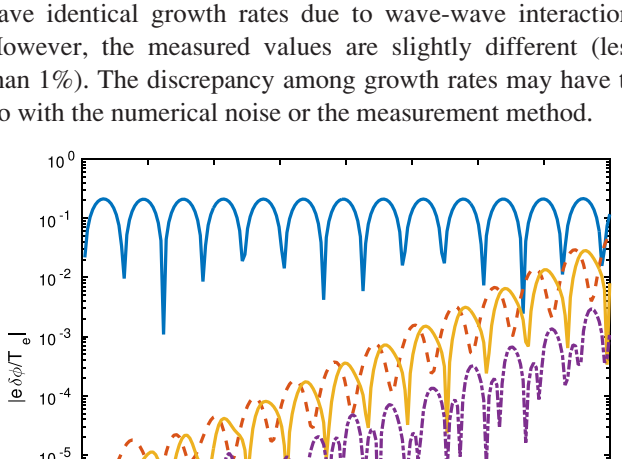

FIG. 1. Time history of scalar potential $\delta\phi$ of the pump wave 202 and daughter waves with the highest amplitudes in the simulation keeping all daughter waves.

TABLE I. Growth rates of the dominant daughter waves generated by pump wave 101 (top 5 rows) and by pump wave 202 (bottom 2 rows).

	γ_{020}/ω_A	γ_{121}/ω_A	γ_{222}/ω_A
Keep all daughter waves up to $k_\alpha = 2$	0.248	0.249	0.247
Keep modes 101, 020, 121, and 222	0.248	0.250	0.250
Keep modes 101, 020, and 121	N/A	N/A	N/A
Keep modes 101, 121, and 222	N/A	0.136	0.137
	γ_{040}/ω_A	γ_{242}/ω_A	γ_{444}/ω_A
Double box sizes keep all daughter waves up to $k_\alpha = 4$	0.241	0.242	0.243

The next step is to set up pump wave with the same wavevector as earlier ($k_x\rho_s = k_\perp\rho_s = 0.2$, $k_y\rho_s = 0$, $k_\parallel\rho_s = 0.002$) and reduce the simulation box size by half. That way, the pump wave energy is limited to transfer to waves with higher **k**, up to 2 wavelengths fitted in each direction in the Cartesian coordinate system. Since the simulation box size is halved, the pump wave is labeled as mode 101. The growth rates of the three dominant modes are listed in Table I, and they are higher by at most 3% compared to the ones from Figure 1. Therefore, even when the pump wave energy is allowed to transfer to waves with longer wavelengths, it preferably cascades to waves with shorter wavelengths in the KAW turbulence.

B. Role of convective cell

To identify which mode plays a dominant role in the nonlinear interactions of KAW, we first filter all the modes except for the pump wave of mode 101, and daughter waves of mode 020, 121, and 222. The time history of the $|\delta\phi|$ of the pump wave and three daughter waves are displayed with solid lines in Figure 2, and the growth rates of the daughter waves are measured and listed in Table I. If we compare the growth rates of the daughter waves in this case with the same waves when all the modes with k_α of up to 2 are kept, they are almost identical. The discrepancy between the growth rates from those two simulations is at most 1.2%.

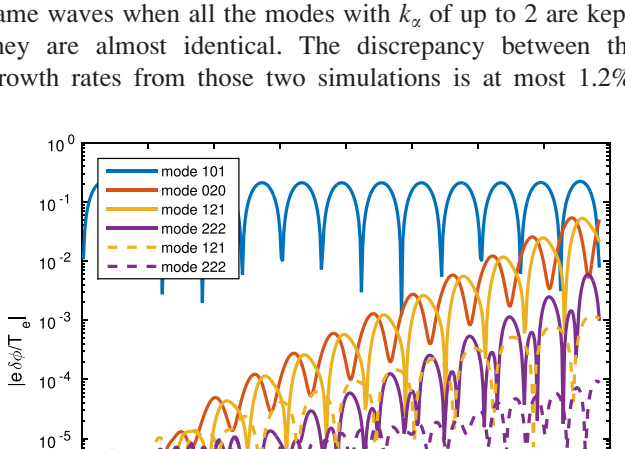

FIG. 2. Time history of the scalar potential $\delta\phi$ of the pump wave 101 and daughter waves. Solid lines represent the simulation in which mode 101, 020, 121, and 222 are kept; while dash lines represent the simulation in which mode 101, 121, and 222 are kept.

Therefore, these three daughter waves were proven to be the ones that received the majority of the energy from the pump wave.

The next step is to determine the importance of each daughter wave in different sets of wave-wave coupling. According to wave-matching condition, mode 101 could couple to daughter waves of modes 020 and 121. Hence, one of the simulation tests we performed is to filter out all the modes except the pump wave of mode 101 and daughter waves of mode 020 and 121. The time history in this case shows that daughter waves would not grow exponentially.

In the other simulation, we filter out all the modes except the pump wave (mode 101) and daughter modes 121 and 222. The time history of the scalar potential of those three modes is displayed with dash lines in Figure 2. This shows that although daughter waves 121 and 222 grow exponentially, the growth rate is less than half of the case when mode 020 is included in the simulation.

In summary, the daughter waves that gained the most energy from the pump wave 101 are modes 020, 121, and 222. The CC (mode 020) enhances energy transfer from the pump wave into the daughter modes. Four waves (101, 020, 121, 222) are required minimal waves to model the energy cascade of a single pump wave (101). A conjecture is that the resonant three-wave interaction of (101, 121, 222) generates the 121 mode, which may provide a sideband for the modulational instability of (101, 121, 020). In addition, these four modes exhibit behavior of standing waves: the time history of all modes are sinusoidal. The real frequency of mode 121 is about the same as the real frequency of the pump wave, which is about $1.03\omega_A$. The amplitude oscillations of mode 020 is due to the pump wave being a standing wave, whose amplitude is oscillating with the wave frequency. On the other hand, the real frequency of mode 222 is approximately twice the frequency of the pump wave.

The CC 020 is composed of zonal density (ESCC) and zonal current (MSCC). The removal of zonal current from mode 020, which turns it into an ESCC, shows a small increase in growth rates; the growth rates of mode 020, 121, and 222 are $\gamma/\omega_A = 0.262$, 0.262 and 0.265, respectively. This shows that, by comparing to the growth rates in Table I, linear MSCC could barely affect KAW wave-wave interaction. Note that the nonlinear part of the MSCC, $\overline{\delta A_\parallel^{NL}}$, is not included in this simulation because Wang has shown that the nonlinear term is not important in the wave-wave interaction.[40]

C. Parametric dependence of convective cell generation

In this section, we scan the pump wave parameters to provide further insights into the CC generation. A scan of the pump wave amplitudes is displayed in Figure 3(a). The perpendicular wavevector $k_\perp\rho_s$ is fixed at 0.2 and parallel wavevector $k_\parallel\rho_s$ at 0.002. A linear fit, $\gamma/\omega_A = 35.08\,|\delta B_\perp/B_0| - 0.17$, is plotted on top of the simulation results, which indicates that the threshold for CC generation is at $\delta B_\perp/B_0 = 0.005$. The linear fit is qualitatively consistent with the theory of modulational instability, in which the zonal

flow can be spontaneously excited by KAW with a growth rate linearly dependent on the wave amplitude, as long as the amplitude is above the threshold value.

A scan of the parallel wavenumbers is displayed in Figure 3(b). The perpendicular wavevector $k_\perp \rho_s$ is fixed at 0.2 and the perturbed magnetic field $\delta B/B_0$ at 0.012. At lower-$k_\parallel \rho_s$ values, γ is independent of $k_\parallel \rho_s$ as expected, since the dominant nonlinear term $v_{E\times B}$ only involves $k_\perp$. The growth rate decreases as $k_\parallel$ increases.

A scan on the perpendicular wavenumber is displayed in Figure 3(c). The parallel wavevector $k_\parallel \rho_s$ is fixed at 0.002 and $\delta B/B_0$ at 0.012. The growth rate's dependency on $(k_\perp \rho_s)^2$ can be fitted into a linear function, $\gamma/\omega_A = 5.90(k_\perp \rho_s)^2$.

D. Generation of convective cell by two pump waves

Considering the importance of CC in the energy cascade of KAW, we now study the generation of CC by two pump waves. This could be the meaningful first step towards the fully nonlinear simulation of the CC interaction with a self-consistently determined KAW turbulence. In this respect, the CC generation by two pump waves is just a variant of the same process with one pump wave only. Nonetheless, there are specific requirements in order for the three-wave interaction to occur. According to the three wave matching condition, the waves have to satisfy the following matching conditions: $\mathbf{k}_1 + \mathbf{k}_2 = \mathbf{k}_3$ and $\omega_1 + \omega_2 = \omega_3$. In addition, the dominant nonlinear term that controls the three-wave interaction shows that $E \times B$ nonlinear term is proportional to $k_{x1}k_{y2} - k_{x2}k_{y1}$. If two pump waves are coherent with suitably chosen perpendicular wave vectors, it could maximize the nonlinear interaction. In our simulation, we use $\sin(k_{x1}x + k_{z1}z)$ as pump wave $(-1, 0, -1)$ and its complex conjugate (1, 0, 1), and $\sin(k_{y1}y + k_{z1}z)$ as pump wave (0,1,1) and its complex conjugate $(0, -1, -1)$. Both of these pump waves have an initial amplitude $\delta B/B_0 = 0.012$ and $k_\perp \rho_s = 0.2$ and $k_\parallel \rho_s = 0.002$. We can use two pump waves $(-1, 0, -1)$ and (0, 1, 1) to beat a CC $(-1, 1, 0)$. The complex conjugates of these waves can also be involved in another set of three-wave interaction. Figure 4 shows the time history of the pump waves and two of the selected CC as daughter waves. Mode $(-1, 1, 0)$ shows a clear exponential growth, and the growth rate of this convective cell is measured to be $\gamma/\omega_A = 0.1$. The complex conjugate of CC $(-1, 1, 0)$ is $(1, -1, 0)$, which is not shown in Figure 4, and its growth rate is identical to $(-1, 1, 0)$. On the other hand, mode (1, 1, 0) has no growth throughout the simulation time window.

We also tested how the growth rate of the convective cell depends on the pump wave parameters. The first pump wave parameter we scanned is the pump wave amplitudes $\delta B/B_0$ for both pump waves, while the wave vectors are fixed. The result is shown in Figure 5(a). The growth rate is linearly dependent on the pump wave amplitudes. We made a linear fit $\gamma/\omega_A = 13.15|\delta B_\perp/B_0| - 0.05$ to the simulation measurements, and we found that the threshold to exponential growth is at $\delta B_\perp/B_0 = 0.004$.

The second parameter scan we tried is the parallel wavenumber $k_\parallel \rho_s$ of the pump waves. While we scan the parallel wavenumber, the amplitudes $\delta B/B_0$ and perpendicular wavenumbers $k_\perp \rho_s$ are fixed. As shown in Figure 5(b), the growth rate decreases as $k_\parallel \rho_s$ increases, at a trend that closely resembles a linear function.

The third parameter scan we tried is the perpendicular wavenumber $k_\perp \rho_s$ of the pump waves. The fixed pump wave parameters in this scan are initial pump amplitudes $\delta B/B_0$ and parallel wavenumbers $k_\parallel$. The growth rate γ/ω_A vs. $k_\perp \rho_s$ is shown in Figure 5(c). The growth rate's relationship with $k_\perp \rho_s$ can be described using a linear function $\gamma/\omega_A = 0.71k_\perp \rho_s - 0.04$. This relationship differs from the single pump wave simulation (see Figure 3(c)).

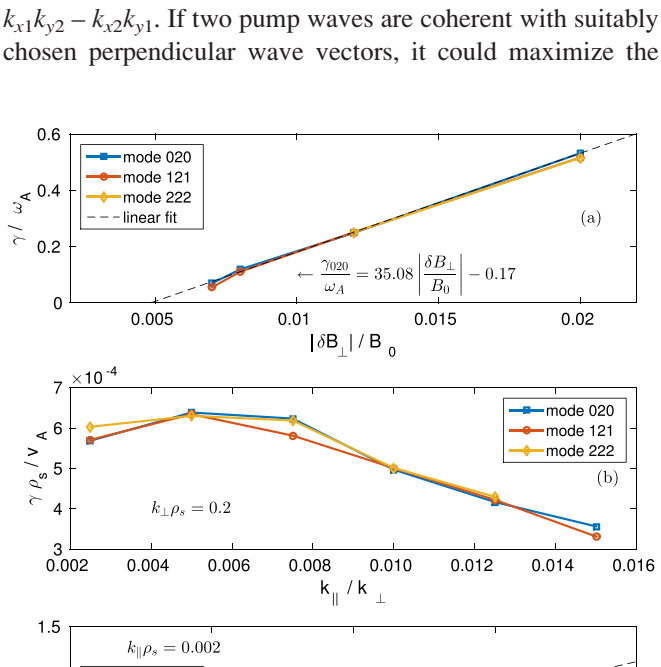

FIG. 3. Growth rates γ/ω_A of daughter waves with respect to the pump wave (a) amplitude $\delta B_\perp/B_0$, (b) parallel wavenumber $k_\parallel$, and (c) square of perpendicular wavenumber $k_\perp^2$.

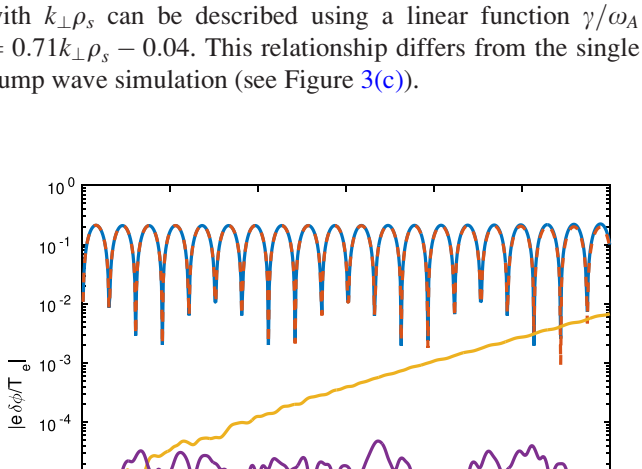

FIG. 4. Time history of scalar potential $\delta\phi$ of the pump waves (1, 0, 1) and (0, 1, 1) along with the daughter waves $(-1, 1, 0)$ and (1, 1, 0).

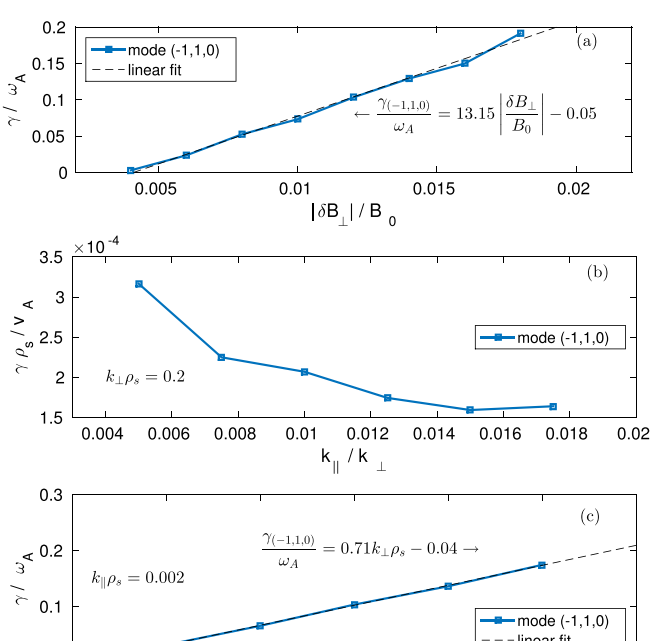

FIG. 5. Growth rates γ/ω_A of mode $(-1, 1, 0)$ with respect to the pump wave (a) amplitude $\delta B_\perp/B_0$, (b) parallel wavenumber $k_\parallel$, and (c) perpendicular wavenumber $k_\perp$.

IV. CONCLUSION

A gyrokinetic ion, fluid electron model to study the convective cell (CC) in nonlinear KAW interaction is presented in this paper. A single KAW transfers its energy mainly to other KAWs with shorter wavelengths. Notably, three daughter waves, among which is a CC, have the strongest interaction with the pump wave. The CC generated by the KAW interaction enhances the energy transfer to the daughter waves by approximately a factor of two. Specifically, the ESCC plays a major role to the enhancement of energy transfer, while MSCC plays a minor role.

In the single pump wave simulations, we observed that the growth rates have a linear dependence on the pump wave amplitude, with a finite threshold. The growth rates also have a linear dependence on the square of the perpendicular wavevector and large-parallel wavevector values. However, the growth rates show no dependence on small-parallel wavevector values. Two pump wave simulations show different parametric dependencies. The growth rates have a linear dependence on both pump wave amplitudes (with a finite threshold) and a perpendicular wavevector.

Further study on the parametric dependence of CC can provide a better understanding on the current simulation results. The ultimate goal of this work is to understand the role of CC in the interaction of multiple KAW leading to perpendicular energy cascade.

ACKNOWLEDGMENTS

This work is supported by the Gates Millennium Scholars Program and by DOE SciDAC GSEP Center. The computational resources utilized for this work is provided by the National Energy Research Scientific Computing Center (DOE Contract No. DE-AC02-05CH11231) and the High Performance Computing Cluster at the University of California, Irvine.

[1]J. W. Bieber, W. Wanner, and W. H. Matthaeus, "Dominant 2d magnetic turbulence in the solar wind," in *Solar Wind Eight: Proceedings of the Eighth International Solar Wind Conference, Dana Point, CA, June 1995* (American Institute of Physics, 1996), Vol. 382, p. 355.
[2]J. J. Podesta, "Dependence of solar-wind power spectra on the direction of the local mean magnetic field," Astrophys. J. **698**, 986 (2009).
[3]J. V. Shebalin, W. H. Matthaeus, and D. Montgomery, "Anisotropy in MHD turbulence due to a mean magnetic field," J. Plasma Phys. **29**, 525–547 (1983).
[4]W. H. Matthaeus, S. Oughton, S. Ghosh, and M. Hossain, "Scaling of anisotropy in hydromagnetic turbulence," Phys. Rev. Lett. **81**, 2056 (1998).
[5]P. Goldreich and S. Sridhar, "Toward a theory of interstellar turbulence. 2: Strong alfvenic turbulence," Astrophys. J. **438**, 763–775 (1995).
[6]A. N. Kolmogorov, "The local structure of turbulence in incompressible viscous fluid for very large Reynolds numbers," Dokl. Akad. Nauk SSSR **30**, 301–305 (1941).
[7]W.-C. Müller and R. Grappin, "Spectral energy dynamics in magnetohydrodynamic turbulence," Phys. Rev. Lett. **95**, 114502 (2005).
[8]B. J. Vasquez, C. W. Smith, K. Hamilton, B. T. MacBride, and R. J. Leamon, "Evaluation of the turbulent energy cascade rates from the upper inertial range in the solar wind at 1 au," J. Geophys. Res.: Space Phys. (1978–2012) **112**, A07101 (2007).
[9]B. K. Shivamoggi, "Magnetohydrodynamic turbulence: Generalized formulation and extension to compressible cases," Ann. Phys. **323**, 1295–1303 (2008).
[10]R. H. Kraichnan, "Inertial-range spectrum of hydromagnetic turbulence," Phys. Fluids (1958–1988) **8**, 1385–1387 (1965).
[11]R. J. Leamon, C. W. Smith, N. F. Ness, W. H. Matthaeus, and H. K. Wong, "Observational constraints on the dynamics of the interplanetary magnetic field dissipation range," J. Geophys. Res. **103**, 4775–4787, doi:10.1029/97JA03394 (1998).
[12]M. L. Goldstein and D. A. Roberts, "Magnetohydrodynamic turbulence in the solar wind," Phys. Plasmas (1994–present) **6**, 4154–4160 (1999).
[13]G. G. Howes, J. M. TenBarge, W. Dorland, E. Quataert, A. A. Schekochihin, R. Numata, and T. Tatsuno, "Gyrokinetic simulations of solar wind turbulence from ion to electron scales," Phys. Rev. Lett. **107**, 035004 (2011).
[14]E. Marsch and C.-Y. Tu, "Evidence for pitch angle diffusion of solar wind protons in resonance with cyclotron waves," J. Geophys. Res.: Space Phys. (1978–2012) **106**, 8357–8361 (2001).
[15]L. Chen and A. Hasegawa, "Kinetic theory of geomagnetic pulsations 1. internal excitations by energetic particles," J. Geophys. Res. **96**, 1503–1512, doi:10.1029/90JA02346 (1991).
[16]L. Chen, Z. Lin, and R. White, "On resonant heating below the cyclotron frequency," Phys. Plasmas (1994–present) **8**, 4713–4716 (2001).
[17]C. C. Chaston, J. W. Bonnell, C. W. Carlson, J. P. McFadden, R. E. Ergun, R. J. Strangeway, and E. J. Lund, "Auroral ion acceleration in dispersive alfvén waves," J. Geophys. Res.: Space Phys. (1978–2012) **109**, A04205 (2004).
[18]H. J. Beinroth and F. M. Neubauer, "Properties of whistler mode waves between 0.3 and 1.0 au from helios observations," J. Geophys. Res.: Space Phys. (1978–2012) **86**, 7755–7760 (1981).
[19]O. Stawicki, S. P. Gary, and H. Li, "Solar wind magnetic fluctuation spectra: dispersion versus damping," J. Geophys. Res. **106**, 8273–8281, doi:10.1029/2000JA000446 (2001).
[20]S. P. Gary and H. Li, "Whistler heat flux instability at high beta," Astrophys. J. **529**, 1131 (2000).
[21]S. Dorfman and T. A. Carter, "Nonlinear excitation of acoustic modes by large-amplitude alfvén waves in a laboratory plasma," Phys. Rev. Lett. **110**, 195001 (2013).
[22]L. Chen and F. Zonca, "On nonlinear physics of shear alfvén waves," Phys. Plasmas (1994-present) **20**, 055402 (2013).
[23]P. K. Shukla, M. Yu, H. Rahman, and K. Spatschek, "Nonlinear convective motion in plasmas," Phys. Rep. **105**, 227–328 (1984).
[24]R. Z. Sagdeev, V. D. Shapiro, and V. I. Shevchenko, "Excitation of convective cells by alfven waves," JETP Lett. **27**, 340 (1978).
[25]O. Onishchenko, O. Pokhotelov, R. Sagdeev, L. Stenflo, R. Treumann, and M. Balikhin, "Generation of convective cells by kinetic alfvén waves in the upper ionosphere," J. Geophys. Res.: Space Phys. (1978–2012) **109**, A03306 (2004).

[26]J. Zhao, D. Wu, M. Yu, and J. Lu, "Convective cell generation by kinetic alfvén wave turbulence in the auroral ionosphere," Phys. Plasmas (1994-present) **19**, 062901 (2012).
[27]A. Lin, J. Dawson, and H. Okuda, "Thermal magnetic fluctuations and anomalous electron diffusion," Phys. Rev. Lett. **41**, 753 (1978).
[28]S. Popel, S. Kopnin, M. Yu, J. Ma, and F. Huang, "The effect of microscopic charged particulates in space weather," J. Phys. D: Appl. Phys. **44**, 174036 (2011).
[29]C. Chu, M.-S. Chu, and T. Ohkawa, "Magnetostatic mode and cross-field electron transport," Phys. Rev. Lett. **41**, 653 (1978).
[30]V. Pavlenko and J. Weiland, "Nonlinear magnetic islands and anomalous electron thermal conductivity," Phys. Rev. Lett. **46**, 246 (1981).
[31]J. Zhao, D. Wu, J. Lu, L. Yang, and M. Yu, "Generation of convective cells by kinetic alfvén waves," New J. Phys. **13**, 063043 (2011).
[32]F. Zonca, Y. Lin, and L. Chen, "Spontaneous excitation of convective cells by kinetic alfvén waves," EPL **112**, 65001 (2015).
[33]Y. Lin, J. R. Johnson, and X. Wang, "Three-dimensional mode conversion associated with kinetic alfvén waves," Phys. Rev. Lett. **109**, 125003 (2012).
[34]L. Chen, Z. Lin, R. B. White, and F. Zonca, "Non-linear zonal dynamics of drift and drift-alfvén turbulence in tokamak plasmas," Nucl. Fusion **41**, 747 (2001).
[35]Z. Lin, T. S. Hahm, W. Lee, W. M. Tang, and R. B. White, "Turbulent transport reduction by zonal flows: Massively parallel simulations," Science **281**, 1835–1837 (1998).
[36]A. J. Brizard and T. S. Hahm, "Foundations of nonlinear gyrokinetic theory," Rev. Mod. Phys. **79**, 421 (2007).
[37]Z. Lin and L. Chen, "A fluid–kinetic hybrid electron model for electromagnetic simulations," Phys. Plasmas (1994–present) **8**, 1447–1450 (2001).
[38]W. W. Lee, "Gyrokinetic approach in particle simulation," Phys. Fluids (1958–1988) **26**, 556–562 (1983).
[39]I. Holod, W. Zhang, Y. Xiao, and Z. Lin, "Electromagnetic formulation of global gyrokinetic particle simulation in toroidal geometry," Phys. Plasmas (1994–present) **16**, 122307 (2009).
[40]Z. Wang, "Gyrokinetic simulation of TAE in fusion plasmas," Ph.D. thesis, University of California, Irvine, 2014.